Proceedings of the 2008 International Manufacturing Science and Engineering Conference
MSEC2008
October 7-10, 2008, Evanston, Illinois, USA

MSEC_ICM&P2008-72210

STRUCTURAL MODIFICATION OF AMORPHOUS FUSED SILICA UNDER FEMTOSECOND LASER IRRADIATION

S. Vukelic
Department of Mechanical Engineering,
Columbia University, New York, NY 10027
sv2147@columbia.edu

B. Gao
Department of Mechanical Engineering,
Columbia University, New York, NY 10027
bg2248@columbia.edu

S. Ryu
Department of Chemistry,
Columbia University, New York, NY 10027
sr2474@columbia.edu

Y.L. Yao
Department of Mechanical Engineering,
Columbia University, New York, NY 10027
yly1@columbia.edu

ABSTRACT

Non-linear absorption of femtosecond laser pulses enables the induction of structural changes in the interior of bulk transparent materials without affecting their surface. This property can be exploited for the transmission welding of transparent dielectrics, three dimensional optical data storages and waveguides. In the present study, femtosecond laser pulses were tightly focused within the interior of bulk fused silica specimen. Localized plasma was formed, initiating rearrangement of the network structure. The change in material properties were studied through employment of spatially resolved Raman spectroscopy, atomic force microscopy and optical microscopy. The nature of the physical mechanisms responsible for the alteration of material properties as a function of process parameters is discussed.

INTRODUCTION

In recent times, advances in femtosecond (fs) laser development have lead to a wide spectrum of new applications [2]. One of main advantages of femtosecond lasers in comparison to nanosecond ones is that they induce much smaller collateral damage due to heat conduction [29]. Furthermore, non-linear absorption, an unique property of femtosecond lasers, makes them particularly suitable for treatment of dielectric materials [4].

Laser assisted transmission welding using conventional nanoseconond (ns) lasers can be utilized when top material is transparent to the laser and bottom material is opaque to it. The laser beam transmits trough the top layer and is absorbed by the opaque material beneath. The subsequent heat accumulation helps to create the weld. When using the ultrafast laser, however, non-linear absorption enables us to induce structural changes into the interior of the target material without affecting the surface. Miyamoto et al. [40] used fs laser to simulate fusion welding by inducing damage within the interior of borosilicate glass. Watanabe et al. [30] investigated conditions to join two substrates using the fs laser. A laser beam was focused on the interface of two transparent substrates resulting in melting and quenching of the surrounding material. Rapid solidification was responsible for joining. Tamaki et al. [32] studied the effect of localized heat accumulation in transmission micro welding. Efforts described above mainly dealt with problems specifically related to welding from a parametric point of view and did not go into details of structural changes that take place within the affected region. Our initial motivation was to gain insight into the welding process. However, this led us to a more fundamental study of the glass – ultrafast laser interaction. Previous studies on this topic are reviewed in the following paragraph.

The potential of creating three dimensional optical storages [25] has led to the study of the interaction of various transparent materials with ultra-fast laser pulses. Glezer and Mazur [26] showed that femtosecond laser pulses tightly focused into the interior of the glass with an energy level near to the threshold produce sub-micron cavities or voxels. These structures are characterized by a change in refractive index and consist of a centrally placed void accompanied by a denser surrounding region. Bellouard et al. [24] studied change in morphology of fused silica through effects of etching selectivity, increase of internal stresses and densification.

Schaffer et al. [27], [28], [29] explored different aspects of ultra-fast laser fused silica interaction. Topics covered included the potential of micromachining bulk glass with use of nanojoule energy, bulk heating of transparent materials and morphology of structural changes induced by femtosecond lasers. Kucheyev and Demos [33] used photoluminescence (PL) and Raman spectroscopy to characterize defects created in the amorphous fused silica irradiated by nanosecond and femtosecond lasers with different wavelengths. Their PL results have shown that laser irradiation causes forming of non-bridging oxygen hole centers (NBOHC) and oxygen-deficiency centers (ODC). Raman spectroscopy revealed densification of irradiated area. Chan et al. [21] used femtosecond laser to irradiate the interior of a fused silica slab and performed in situ Raman spectroscopy measurements. Atomic-scale structural changes were observed that lead to the densification of affected material. Damage induced was related to changes in other properties obtained for vitreous silica using different treatments.

The work reviewed above addresses change in properties and morphology which are a consequence of structural alterations due to the ultra-fast laser irradiation of interior of transparent materials. It also somewhat explains the physical process that leads to those changes. In the study presented here, the focus is on the atomistic level and rearrangement of the ring structures of which amorphous fused silica consists. Spatially resolved Raman spectroscopy is employed as a non-destructive characterization technique to show local densification and relative volume fraction change of ring structures within focal volume and in the surrounding region. Moreover, the contribution of different mechanisms in feature formation under more complex process conditions is examined. In particular, thermal and explosive plasma expansion mechanisms are studied.

FEMTOSECOND LASER IRRADIATION OF TRANSPARENT DIELECTRIC MATERIALS

The mechanism of femtosecond laser interaction with both metals and dielectric materials has been studied intensively in recent times [4], [1], [34]. Unlike linear photon absorption that follows Beer-Lambert law seen in nanosecond pulse regime, the absorption of laser energy with pulse duration in order of femtoseconds is done through nonlinear absorption, and it is independent from the laser wavelength. This phenomenon enables the creation of features within interior of the bulk specimen without affecting its surface. In the next paragraph the principle of interaction of ultrafast lasers with dielectrics will be briefly reviewed.

At femtosecond pulse regime (pulse duration ~ 100 fs) ionization of dielectric material occurs at the beginning of the pulse followed by the absorption of laser energy by free electrons through inverse Brehmstrahlung and resonance absorption mechanism [1]. The pulse duration is shorter than plasma expansion and heat conduction time, resulting in the feasibility to ionize any material. Furthermore, the main process that occurs during that time is heating of the electrons by the laser field. Depending on the laser intensity, two competing mechanisms are responsible for the absorption of the femtosecond laser energy. At lower laser intensities, below 10^{12} W/cm^2, avalanche ionization takes place, whereas at intensities above 10^{13} W/cm^2 multiphoton ionization is responsible for absorption. In the case of avalanche ionization, upon absorption of photons at lower intensity, kinetic energy of free electrons becomes sufficiently high to trigger collision impact ionization of the target material. That leads to the generation of more free electrons through the process in which free electron density increases. On the other hand, multiphoton ionization occurs when a number of electrons with energy hν and wavelength collide with the bound electron at the same time. If the total energy of absorbed photons is greater than ionization potential, electron breaks free from the valence.

Through processes described above, free electron density rises until it reaches critical value. Ionization of transparent dielectric material occurs at the beginning of the pulse followed by the absorption of laser energy by free electrons via inverse Brehmstrahlung and resonance absorption mechanism [1]. Due to this transparent materials become completely opaque [4]. Furthermore, material in the focal volume is transformed into plasma with metallic properties through laser induced breakdown. Subsequent processes are the consequence of plasma-matter interaction.

In the field of femtosecond glass interaction, a lot of work has been conducted by Mazur's group at Harvard University. The initial motivation for their work was the potential of creating three dimensional data storages as well as waveguides. They showed [25], [26] that single femtosecond laser pulse can create a void inside of bulk transparent specimen surrounded by the densified shell. The mechanism responsible for creation of these structures is explosive plasma expansion. When ultrafast laser pulse energy is deployed into the sample, high temperature and pressure initiate formation of optically dense electron-ion plasma. The material in the center of the focal volume is then ejected into the surrounding area creating a voxel or less dense region. On the other hand, when multiple pulses applied at the same position nature of laser-transparent dielectric interaction becomes thermal [28]. For high-repetition-rate pulsing (~MHz), and nanojoule energy of the pulses, characteristic thermal diffusion time in glass is longer than the time between two pulses leading to thermal accumulation, which has the consequence of denisfying affected region. A similar approach can be used at lower repetition rates (~kHz) and microjoule pulse energies [37].

Another important parameter in determining morphology, structure and size of the altered region is the numerical aperture (NA) of the objective used to focus incoming laser beam [28], [29]. For Gaussian beams focal volume has the shape of Gaussian ellipsoid and its size is a function of numerical aperture [5]. Intensity distribution within the focal volume is:

$$I = \exp[(-2(x^2 + y^2)/\omega_{xy}^2)]\exp[-2z^2/\omega_z^2] \quad (1)$$

Where x, y and z are coordinates and ω_{xy} and ω_z are diameters of the ellipsoid defined by

$$\omega_{xy} = \frac{0.325\lambda}{NA^{0.91}}$$
$$\omega_z = \frac{0.532\lambda}{n_i - \sqrt{n_i^2 - NA^2}} \quad (2)$$

where λ is laser wavelength and n_i is refractive index. With the fixed laser energy smaller NA will cause loose focusing in which produced plasma is not energetic enough to drive

explosive expansion. This will result in a larger affected area with small refractive index change in irradiated area. In contrast, tight focusing has effect of producing cavity surrounded with densified material as described above.

Formation of Ring Structures in Fused Silica

One of the main characteristics of amorphous solids is the lack of regularly repeating groups of atoms which are native to the crystalline materials. Amorphous fused silica belongs to the group of so called associated liquids [6] which form bonds in definite vectorial positions in space, leading to the formation of ring structures that connect molecules. Ring distribution can further be defined via shortest path analysis. In this method, an oxygen atom is connected to two silicon atoms in the path such that the smallest possible ring is formed [6], [9]. In the case of amorphous solids, these rings then form a random network. A random network of atoms in fused silica can be seen on Figure 1. In fused silica, ring structures consist of tetrahedral atomic arrangements, suggesting that basic structural unit of such amorphous materials is tetrahedron.

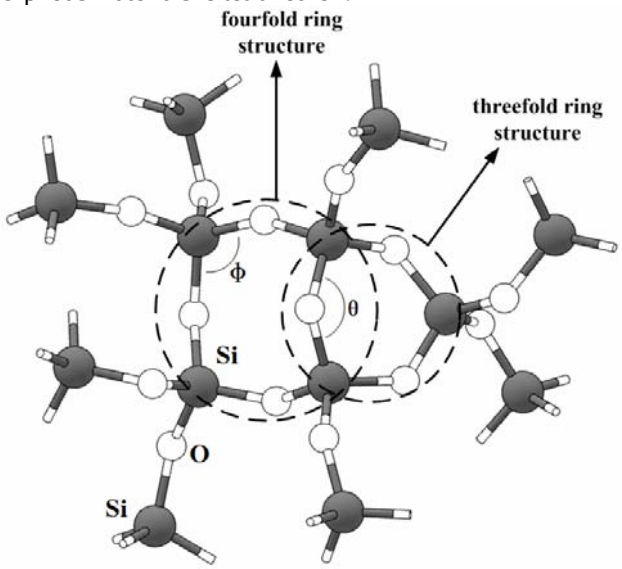

Figure.1 Ball and stick model of the random network in the fused silica. Encircled are three-fold and four-fold ring structures.

Due to a lack of theory that would connect properties at the micro and macro scale, the structure of glasses is analyzed through the creation of statistical models. Two types of models can be found in the literature. In the first model, silicon and oxygen atoms are represented by spheres connected with wires [8]. This model is idealized in the sense that it does not take into account defects or impurities. The second model is based on atomic interactions. This model relies on statistical mechanics and interactions are more recently [9], [20] governed by molecular dynamics method.

Employing molecular dynamic methods, one can gain insight of fused silica network through discussion of n-fold rings. The basic structural unit consists of silicon atom surrounded by four oxygen atoms. There are six different ways to form closed path starting from structure denoted as O_1-Si_1-O_2 and one looks for the shortest path to form a ring. Statistical analysis is used to calculate n-fold rings.

Most of the ring structures contain five or six ring members. This is due to the fact that angle between O-Si-O bonds are approximately 109^o, suggesting that larger ring structures are formed from almost perfect tetrahedrons which require minimal strain energy for their formation. In contrast, the formation of three and four member rings requires smaller O-Si-O angle (around 102^o) which has a consequence in distorting tetrahedrons that create these ring structures. Thus strain energy required for formation of these rings is higher than for formation $n \geq 5$.

EXPERIMENTAL SETUP AND CHARACTERIZATION

Amplified Ti-Sapphire laser system Spectra-Physics Hurricane with pulse duration of 130 fs at 1 kHz repetition rate and 800 nm wavelength was used to conduct experiments. Zeiss Plan Neofluar 40x objective lens with NA 0.65 was employed to focus the laser, providing approximately 1.5 μm spot size. The beam was focused into the interior of the 1.6 mm thick, 20 mm square S1-UV grade fused silica glass specimen mounted on the Aerotech motorized linear stage to create localized structural changes. A schematic diagram of the experiment setup can be seen in Figure 2. A number of different conditions were applied by varying feedrate of the stage and energy of the laser pulses. Pulses were applied at energies ranging from 2 μJ to 35 μJ and stage velocities varied from 0.04 mm/s to 1 mm/s.

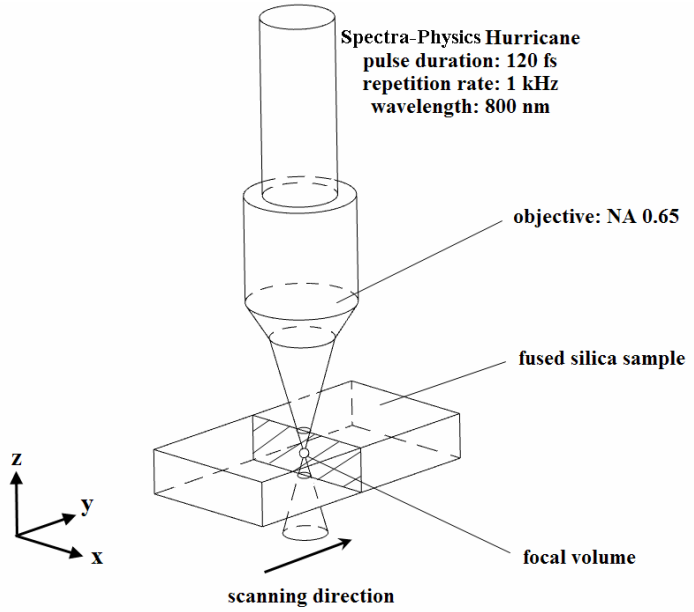

Figure.2 Schematic of experimental setup. The shadowed plane (cross section) shows that the laser beam is focused to the interior of our fused silica sample. Laser beam scanning direction is along the y axis

After treatment, the affected region was examined via micro-Raman spectroscopy to characterize structural changes. Raman spectra was obtained in a back scattering geometry using 40x objective with correction collar which compensated optical aberrations caused by intervening fused silica material. The excitation wavelength was 514.5 nm (Ar ion laser) and the laser power at sample was 14 mW. To spatially filter out scattering and luminescence from other than focal volume, a 50μm pinhole was placed in front of the spectrometer. The spectral resolution was found to be 8 cm^{-1}. Spatial mapping of the cross-section was performed with 1 μm spacing in the x

direction and 5 μm spacing in z direction. The sample was then sectioned, carefully polished with cerium-oxide and cross-section observed with transmission light optical microscope. Cross-section surface was mapped employing atomic force microscopy (AFM).

Raman Spectroscopy in AX_2 Glasses

Raman scattering can be observed as modulation of the dipole moment induced by molecular vibrations. Scattering is the result of forced oscillations of the dipole moment generated by the electromagnetic field of the incident light [35]. In the following paragraphs, a brief description of the nature of Raman spectroscopy in AX_2 glasses will be presented.

The structure and vibrational properties of glasses have been studied theoretically and experimentally. A theoretical approach through employment of central force model was introduced by Sen and Thorpe [7]. The model studies vibrational densities of AX_2 glasses such as SiO_2, GeO_2 etc., which consist of a random network made of linked tetrahedra. Bond distances between the atoms in tetrahedra are the same, and the bond angle in the AXA bridge, represented by θ, is constant for the entire network. According to the model, the structure does not necessarily create a ring of bonds. Assuming non-central forces are negligible and central force α (bond-stretching) is constant, [7] used potential energy

$$V = \frac{\alpha}{2}\sum_{\langle ij \rangle}\left[\left(\vec{u}_i - \vec{u}_j\right)\cdot \vec{r}_{ij}\right]^2 \tag{3}$$

and equations of motion of bonds

$$\begin{aligned}
\left(M\omega^2 - \alpha\right)u_1 &= -\left(\alpha \sin\frac{\theta}{2}\right)\alpha - \left(\alpha\cos\frac{\theta}{2}\right)y \\
\left(m\omega^2 - 2\alpha\sin^2\frac{\theta}{2}\right)x &= -\left(\alpha\sin\frac{\theta}{2}\right)u_1 + \left(\alpha\sin\frac{\theta}{2}\right)u_2 \\
\left(m\omega^2 - 2\alpha\cos^2\frac{\theta}{2}\right)y &= -\left(\alpha\cos\frac{\theta}{2}\right)u_1 - \left(\alpha\cos\frac{\theta}{2}\right)u_2
\end{aligned} \tag{4}$$

where u_i and u_j are displacements, $\boldsymbol{r}$ is unit vector in the direction of the bond, m and M are the mass of atom X and A respectively and is ω_i are angular frequencies. Derived [7], vibrational states as a function of intertetrahedral angle θ are:

$$\begin{aligned}
\omega_1^2 &= (\alpha/m)(1+\cos\theta) \\
\omega_2^2 &= (\alpha/m)(1-\cos\theta) \\
\omega_3^2 &= \omega_1^2 + (4\alpha/3M) \\
\omega_4^2 &= \omega_2^2 + (4\alpha/3M)
\end{aligned} \tag{5}$$

Furthermore, the motion of each frequency is decomposed into bending, stretching and rocking component following notation of [8]

Galeener [39] developed a method for analyzing Raman spectra of AX_2 tetrahedral glasses based on a central-force network model and compared experimental and theoretical results. He argued that origin of the dominant Raman peak at 440 cm^{-1} (Fig. 3) in the case when incident and scattered light polarization vectors are parallel (HH) corresponds to the lowest-frequency limit ω_1. Moreover, ω_1 corresponds to the pure bending of X atom and is consistent with the experimental observation that Raman scattering mostly arises from changes in bond length and ω_2 is related to the out-of phase stretching.

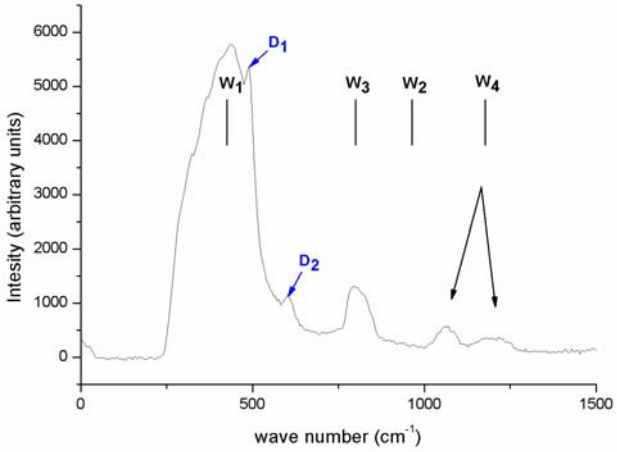

Figure.3 Raman spectra of as received fused silica sample

Theoretical studies have shown that unit tetrahedra SiO_4 in fused silica glass organize themselves into a random network of ring structures, as discussed in previous section. In Raman scattering, different bands correspond to the different n-membered rings. Sharma et al. [17] argued that 440 cm^{-1} band belongs to the six- membered rings and presence of five-, seven- and higher member rings is responsible for broadening of this band. Moreover, shoulder at 490 cm^{-1} is attributed to the four-member ring structure and presence of 606 cm^{-1} peak is due to the wrong-bond or broken-bond defects. [13], [16] argued that 495 cm^{-1} and 606 cm^{-1} lines, which he denoted as D_1 and D_2, can be associated with in-phase breathing motions of oxygen atoms in three- and four- member rings, respectively.

RESULTS AND DISCUSSION

Mechanisms Responsible for the Feature Generation

Optical Micrographs of the Cross-section

Figure 4 shows a cross section of the femtosecond irradiated fused silica sample. Ten different sets of energy levels starting from 2 μJ at the far left to the 35 μJ at the most right side have been introduced into the specimen interior. Within each set there are twelve different conditions varying feedrate from 0.04 mm/s to 1 mm/s. The distance between lines is about 35 μm and there is no interference between treated regions. It can also be seen from Figure 4 that the structural modifications induced are about 400 μm away from the top surface towards the interior of the sample and that material between surface and features is not affected. Figure 5 depicts a cross section of the features produced with 30 μJ laser pulse energy at various feedrates. These features display a teardrop shape, similar to those observed elsewhere [40]. This can be attributed to the geometry of the focal volume which follows the Gaussian ellipsoid. Furthermore, it can be seen that feature width is strongly dependent on the scanning speed which is proportional to the amount of overlapping between pulses. At the same time, the height of the features does not change much. At lower federates, two regions within the feature can be distinguished [40].

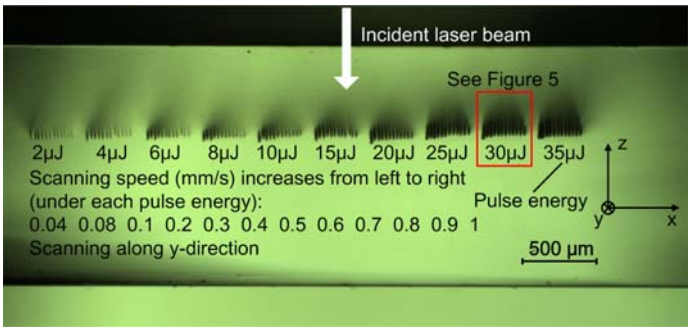

Figure.4 Optical microscopy of cross section view (x-z plane) of femtosecond-laser-irradiated fused silica at different energy levels (from 2 μJ up to 35 μJ) and scanning speeds (from 0.04mm/s up to 1mm/s for each energy level). Scanning is along y direction, perpendicular to the cross section x-z plan. The sample was cross-sectioned and polished after experiment

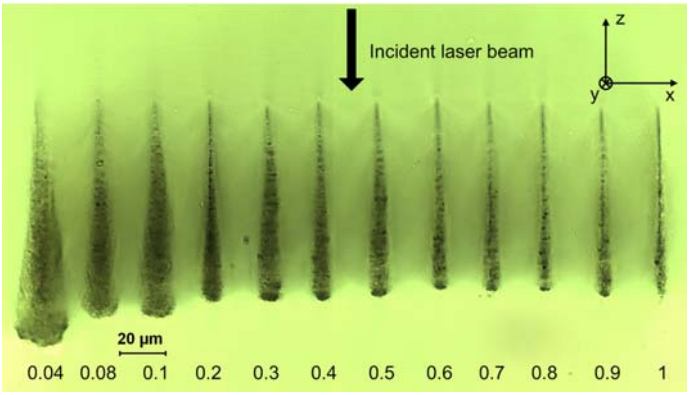

Figure.5 Optical micrograph of cross section of femtosecond laser-irradiated fused silica sample with 30 μJ laser pulse energy. Features correspond to different scanning speeds (mm/s)

The inner region might correspond to the material melted in the focal volume [28], based on the assumption that femtosecond laser energy deposited within focal volume at low stage velocities behave as moving heat source. The formation of the outer region is a consequence of heat conduction between the inner region and surrounding material. At higher feedrates, it can be observed that the resulting feature is narrower, and that instead of a relatively broad inner region, only a sharp line in the middle of the teardrop can be seen. One explanation might be that as the stage speed increases, the amount of overlapping decreases, and as a result, the feature generating mechanism is less thermal in nature. The amount of heat transfer between the focal volume and surrounding area decreases, results in narrower feature. Further, explosive plasma expansion upon single femtosecond laser pulse creates voids surrounded by denisified material [25], [26]. When overlapping is not significant explosive plasma expansion mechanism might be responsible for feature generation. This implies that sharp lines in the middle of the features observed at higher scanning speeds are actually voids. This will be shown in the next section.

Atomic Force Microscopy of the Cross-section

As discussed in the previous section, at higher feedrates the mechanism responsible for the feature generation is explosive plasma expansion. This mechanism is athermal in nature and as

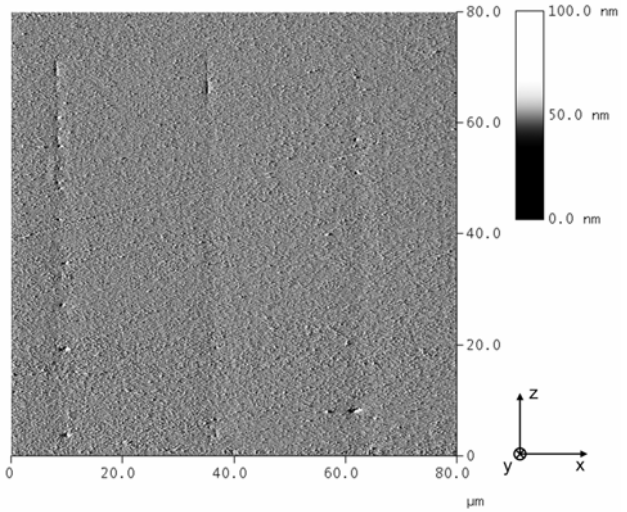

Figure.6 AFM cross section topography of laser-irradiated fused silica sample. The three lines (from left to right) shown in the figure correspond to scanning speeds of 0.8, 0.9 and 1 mm/s with the same 30 μJ laser pulse energy

a result it creates cavities surrounded by the densified material within the interior of bulk specimen. If overlapping between pulses is smaller than a certain critical threshold, the above mechanism will apply and femtosecond laser pulses will generate cavities. Figure 6 shows a cross section area of the fused silica sample scanned via AFM. Features shown are created 30 μJ laser pulse energy and feedrates 1.0 mm/s, 0.9 mm/s and 0.8 mm/s. From the figure it can be seen that laser pulses actually created cavities that correspond to the sharp dark lines seen on the optical micrographs of the cross-section. Due to the periodical nature of the generated structures, it is not meaningful to compare depths of the features because they are dependent on the cross section and it is practically impossible to precisely control the sectioning of the sample. Several different sections have been scanned and cavities have been observed in most of them. Other conditions have been scanned as well but they have not reveal presence of the cavities, which support hypothesis of the thermal nature of the structure formation at lower feedrates.

Further Discussions of the Mechanisms Responsible for Feature Generation and Periodic Nature of the Induced Structures

The features produced in the bulk specimen have the shape of the continuous line. However, its structure at higher feedrates is rather periodic. Figure 7 shows the side view of the femtosecond laser generated lines captured using transmission diffraction interference contrast (DIC). Two different conditions are shown in the figure, created with the same laser pulse energy (30 μJ), but different feedrates, 0.04 mm/s and 1 mm/s, respectively. Slight discrepancy in feature size between cross section and side view comes from the fact that at high magnification depth of field of objectives is very small and the feature is three dimensional thus it is possible to focus a fraction of its size. At slowest stage velocity (Fig. 7 (a)), the line is continuous, quite homogeneous and the feature appears to be created via melting and resolidification. Figure 7 (b) shows the case with 1 mm/s feedrate. Two distinctive regions can be distinguished, the lower of which corresponds to the

wider portion of the teardrop shape in cross section, and the upper one that corresponds to the tail of the teardrop. Narrow, elongated white regions encircled by dark edges represent cavities [29] surrounded by densified material and can be seen in cross section (Figure 6) as a narrow dark line. Some periodicity at stage velocity of 1 mm/s can be observed. Also, interaction between adjacent cavities is observed, which will be subject of future work.

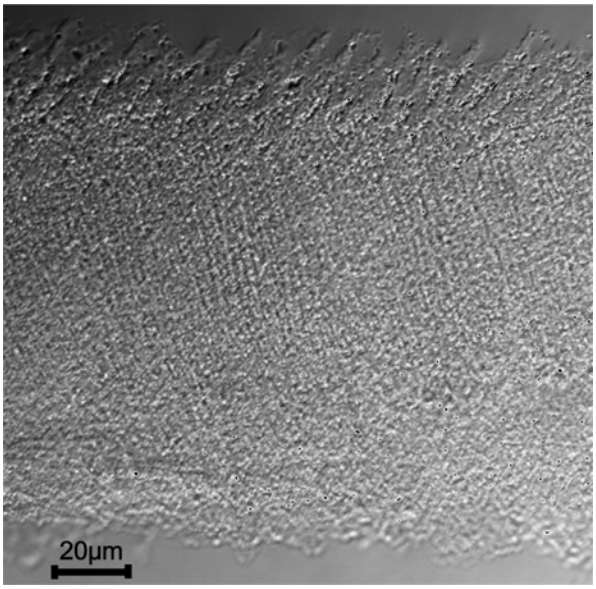

(a)

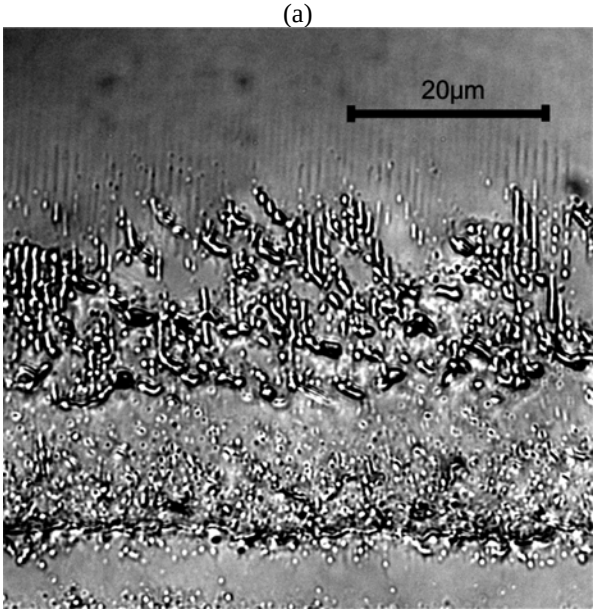

(b)

Figure.7 DIC optical micrograph - side-view (y-z plane) of femtosecond laser irradiated fused silica sample. Laser pulse energy is 30 μJ and two different scanning speeds are shown. (a) scanning speed 0.04mm/s (b) scanning speed 1mm/s

A crude explanation of the periodic behavior is as follows. If we assume that laser intensity at the certain spatial position follows Gaussian distribution of the laser beam spot in the case of the feedrates higher than 1.5 mm/s, when there is no overlapping, intensity as function of the laser path is periodic with the pitch corresponding to the distance between laser pulses. In the case of 1 mm/s federate, due to the partial overlapping of the laser pulses, the pitch is smaller, about 1 μm, which corresponds to the distance between cavities, observed in Figure 7. Due to the superposition of the normalized intensities produced by the laser pulses there is a threshold intensity that every point in the laser path receives. With a decrease of scanning speed this threshold increases and the spikes which are a consequence of Gaussian intensity distribution decrease, leaving the spatial distribution of energy received by the sample flat. Furthermore, the total amount of energy received by a point on the laser path increases twenty times from no overlapping between pulses to 95% overlapping. In the intermediate case, when there is 33% overlapping, the condition that corresponds to 1 mm/s feedrate, spiked regions receive only one pulse and that is where cavities are likely to be formed.

Modification of Structure of Random Network in Fused Silica

The molecular structure of the fused silica was studied through employment of Raman scattering. Different vibrational bands have been associated with particular ring structures in random network configuration as described in previous sections. Altering its structure has been studied via utilization of Neutron bombardment. It is reported that densification of the fused silica glass has been observed in neutron irradiated samples. Bombardment with neutrons causes different response of 440 cm^{-1}, 495cm^{-1} and 606 cm^{-1} bands which is associated with conversion of five- six- and other higher-membered rings into four-membered rings [17]. Fictive temperature increase has an effect on the increase of the intensity of the 490 cm^{-1} and 606 cm^{-1} bands, [11] suggesting that higher density structure is responsible for these modes. More recently, Chan et al. [22] used Raman scattering to investigate effects of femtosecond laser irradiation of interior of the fused silica. They showed that ultrafast laser treatment causes a relative intensity increase of 495cm^{-1} and 606 cm^{-1} bands with respect to the main peak (440 cm^{-1}), and showed that this increase is a function of the incident laser energy. Area under the increased peak is qualitatively associated with densification of the material. Here a more detailed analysis of Raman scattering of fused silica specimens previously treated by ultra fast lasers was performed. A new method to quantitatively determine percentage of different ring structures within the probed volume is proposed below.

Decomposition of Raman Spectra

The region of interest in Raman spectra obtained from the fused silica sample irradiated with femtosecond laser lies between wavenumbers 300 cm^{-1} and 630 cm^{-1}. Three distinctive peaks were observed in that region corresponding to the different ring structures. It is assumed that vibrational bands in the irradiated volume give the same Raman scattering. The line profiles of the bands are Lorentzians [21], and the broadening of the main (440 cm^{-1}) peak is associated with the presence of higher order ring structures [17]. Due to the statistically small content of the higher memebered ring structures [9], [12] this broadening is neglected and the 440 cm^{-1} peak is approximated as Lorenzian. It is assumed that within the volume of interest four different structures coexist three- four- and five- and six-memebered rings. Furthermore, integrated intensity under Raman peaks corresponding to the structures mentioned above corresponds to percentage volume fraction within the probed volume.

Decomposition of the spectrum was done through a curve fitting process. The non-linear curve fit was done employing Levenberg-Marquardt algorithm. Fitting function was composed by superposing three Lorentz functions with constraints imposed by peak position, as seen in Figure 8. Width, height and area under the peaks were treated as free parameters. Initial guesses for the variables related to the 495 cm^{-1} and 606 cm^{-1} bands were taken from the analytical results found in references [12]. Initial guess for variables associated with 440 cm^{-1} peak were found through fitting of this part of the Raman spectrum as single Lorenzian because the main peak is three orders of magnitude larger than D_1 and D_2 peaks. Decomposition of the Raman spectra is depicted in Figure 8. The total integrated intensity under main, D_1 and D_2 peaks was assumed to correspond to the 100 percent of the ring three- four- and five- and six-fold rings within probed volume. Furthermore, ratio between total integrated intensity and integrated intensity of the particular n-fold rings gave us percentage of that ring structure in the probed volume.

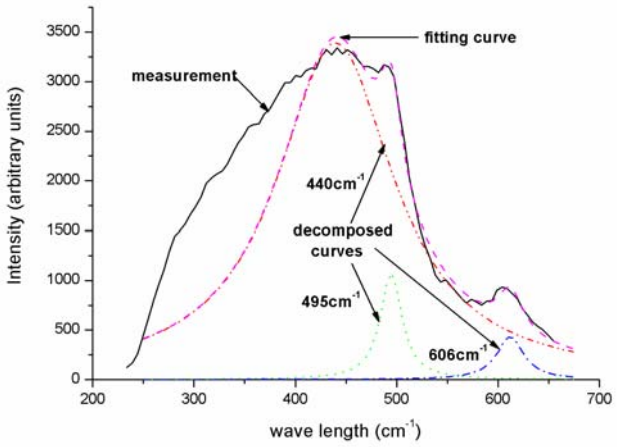

Figure.8 Curve fit and decomposition of the typical Raman spectra in the fused silica

Cross Sectional Contour Maps of Raman Spectra

Figures 9, 10 and 11 depict cross section contour maps of the change in the five- and six-, four- and three-fold ring members, respectively, for the condition of laser pulse energy 30 μJ and feedrate 1 mm/s. The contour map is displayed on the left side and line graphs on the right depict the percentage change of the given n-fold rings for few different z locations. The figures show that shape and size of affected region is consistent with cross sectional optical micrographs. It should also be noted that in unaffected area percentage of n-fold rings is similar to the prediction of the molecular dynamics model used by [9]. Their model predicts about 1 percent of three-membered rings and 8 percent of the four-membered rings in the equilibrium condition. Our experimental findings give approximately 0.8 and 5 percent of three- and four-membered rings, respectively.

From Figure 9 (a) it can be seen that the content of higher order membered rings decreases from 96 percent in untreated region to 83 percent in the center of the focal volume where laser intensity is highest. Also it should be noted that two regions can be distinguished, inner where content of the five-

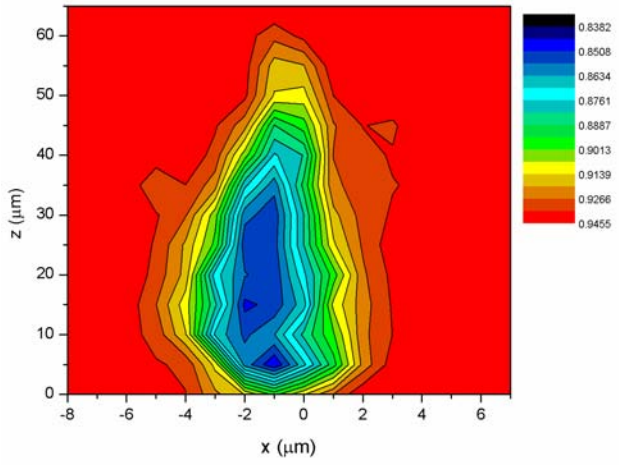

(a)

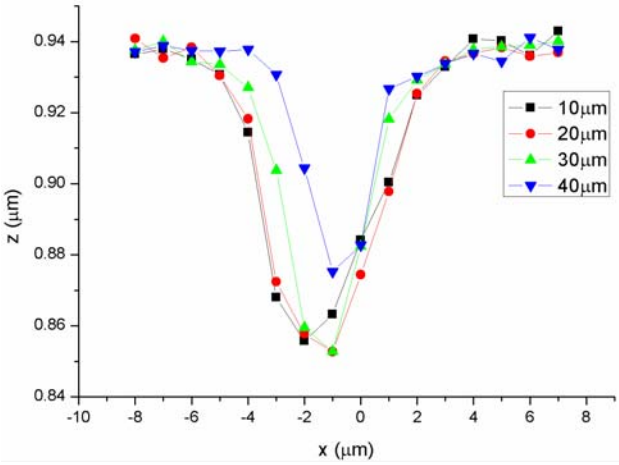

(b)

Figure.9 Percentage presence of 5- and 6- fold rings in fused silica within laser-irradiated region (at laser pulse energy 30 μJ and feedrate 1mm/s). (a) Cross section 2D contour map (b) line plot of percentage change in the region of interest, at different cross-section positions: 10 μm, 20 μm, 30 μm and 40 μm

and six-fold ring members is lowest and constant and outer where it gradually increases to the equilibrium value. Similar distribution can be observed in the three- and four- membered ring contour maps (Figures 10 (a) and 11 (a)). Inner region might be associated with the focal volume, where change is abrupt due to rapid solidification, leaving material frozen and outer would in that case be surrounding affected region. Distribution in contour maps depicting three- and four-membered rings show that content increases from initial 0.8 percent to highest 7 percent for three-fold rings and from 5 to 8.5 percent for the four-fold rings. Also it should be noted that four-fold rings contour map shows that modified area is narrower and shorter than in cases of three- and five- and six-fold rings, suggesting that higher intensity is necessary to alter existing structure into the four membered rings. An analogous observation is made in amorphous fused silica treated by neutron irradiation where it is shown that intensity of 606 cm-1 band increases at faster rate than 495 cm^{-1} [17].

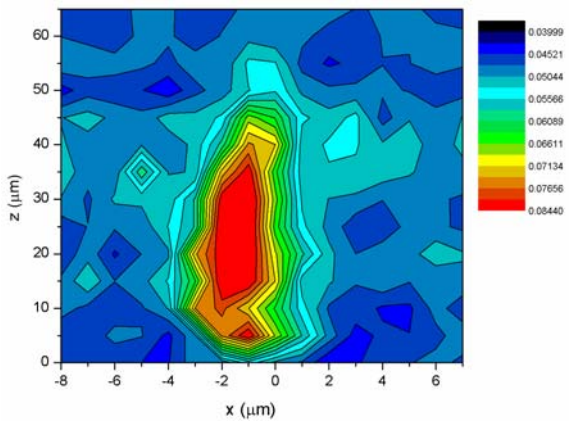

(a)

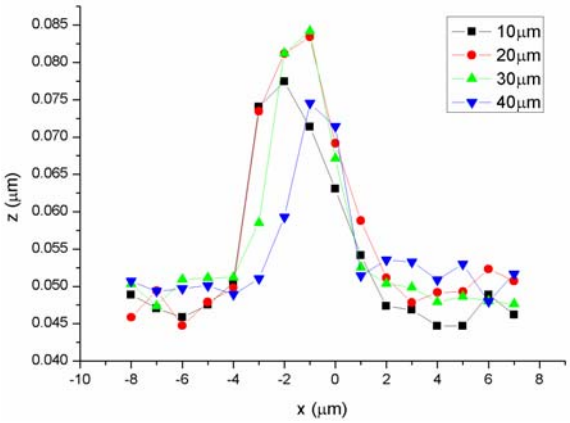

(b)

Figure.10 Percentage presence of 4- fold rings in fused silica within laser irradiated region (at laser pulse energy 30 μJ and feedrate 1mm/s). (a) Cross section 2D contour map (b) line plot of percentage change in the region of interest, at different cross-section positions: 10 μm, 20 μm, 30 μm and 40 μm

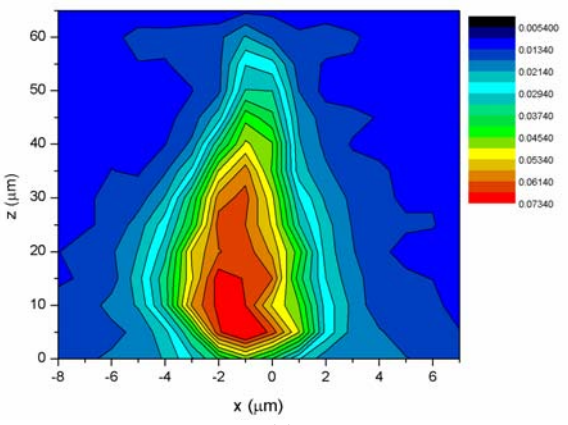

(a)

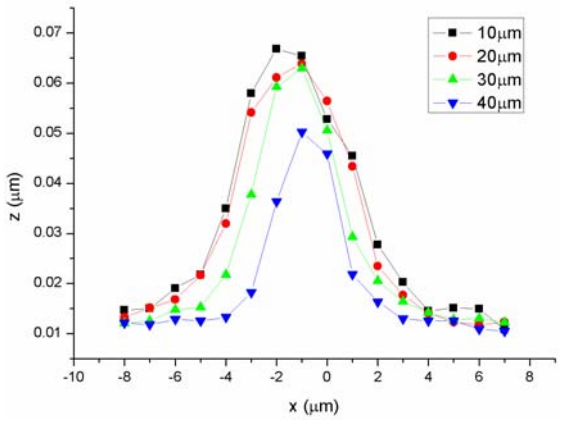

(b)

Figure.11 Percentage presence of 3- fold rings in fused silica within laser irradiated region (at laser pulse energy 30 μJ and feedrate 1mm/s). (a) Cross section 2D contour map (b) line plot of percentage change in the region of interest, at different cross-section positions: 10 μm, 20 μm, 30 μm and 40 μm

CONCLUSION

Structural changes and morphology of amorphous fused silica under ultrafast laser irradiation have been investigated employing Raman scattering, optical microscopy and atomic force microscopy. Two different feature generation mechanisms, based on process conditions have been explored and potential explanation for transition between two regimes given. A new quantitative method for analysis of structural rearrangement of ring structures has been proposed and our experimental findings have been compared with existing models. With proposed method we are able to calculate percentage of n-fold ring structures within the probed volume and comparison of measurements done on the as received fused silica samples with molecular dynamic model showed good agreement.

ACKNOWLEDGMENTS

This work was supported by National Science Foundation under grant DMI-0620741. Authors would like to thank Prof. John R. Lombardi of City University of New York and Dr. Tommaso Baldacchini of Newport/Spectra–Physics for useful discussions. Assistance in preparing figures by Mr. Haohao Jiao is also gratefully acknowledged.

REFERENCES

[1] Gamaly, E.G, Rode, A.V. Luther-Davies, B., Tikhonchuk, V.T., (2002) “Ablation of Solids by Femtosecond Lasers: Ablation Mechanism and Ablation Thresholds for Metals and Dielectrics’, Physics of Plasmas,” Vol. 9, No. 3, pp. 949-957.

[2] Gamaly, E. G., Tikhonchuk, V. T., (1989) “Effect of Ultrashort Light Pulses on a Substance,” Pis’ma Zh. Eksp. Teor. Fiz. 48, No. 8, pp. 413-415.

[3] Shirk, M. D., Molian, P. A., (1998) “A review of Ultrashort Pulsed Laser Ablation of Metals,” Journal of Laser Applications Vol. 10, No. 1, pp. 18-28.

[4] Jiang, L., Tsai, H. L. (2003) “Femtosecond Lasers Ablation: Challenges and Opportunities”, NSF workshop on “Unsolved Problems and Research Needs in Thermal Aspects of Material Removal Processes,” June 10-12, Stillwater, OK

[5] Iyer, V., Rossow, M. J., Waxham, M. N., (2004) “Focal Volume Characterization Using Multiphoton Fluorescence Correlation Spectroscopy (MP-FCS),” Proceedings of SPIE Vol. 5323, pp. 156-159.

[6] King, S., (1967) “Ring Configuration in a Random Network Model of Virteous Silica,” Nature, Vol. 213, pp. 1112-1113.

[7] Sen, P. N., Thorpe, M. F., (1977) "Phonons in AX2 Glasses: From Molecular to Band-like Modes," Physical Review B, Vol. 15 No. 8, pp. 4030-4038.

[8] Bell, R. J., Dean, P., (1966) "Properties of Virteous Silica: Analysis of Random Network Models," Nature, Vol. 212, pp 1354-1356.

[9] Rino, J. P, Ebbsjo, I., (1993) "Structure of Rings in Virteous SiO_2," Physical Review B, Vol. 47, No. 6, pp. 3053-3062.

[10] Galeener, F. L., Barrio, R. A., Martinez, E., Elliot, R. J., (1984) "Vibrational Decoupling of Rings in Amorphous Solids," Physical Review Letters, Vol. 53, No. 25, pp. 2429-2432.

[11] Geissberger, A. E., Galeener, F. L., (1983) "Raman Studies of Virteous SiO_2 Versus Fictive Temperature," Physical Review B, Vol. 28, No. 6, pp. 3266-3271.

[12] Pasquarello, A., Carr, R., (1998) "Identification of Raman Defect Lines as Signatures of Ring Structures in Vitreous Silica," Physical Review Letters, Vol. 80, No. 23, pp. 5145-5147.

[13] Martin, R. M., Galeener, F. L., (1981) "Correlated Excitations and Raman Scattering in Glasses," Physical Review B, Vol. 23, No. 6, pp. 3071-3081.

[14] Laughin, R. B., Joannopoulos, J. D., (1977) "Phonons in Amorphous Silica," Physical Review B, Vol. 16, No. 6, pp 2942-2952.

[15] Galeener, F. L., (1982) "Planar Rings in Glasses," Solid State Communications, Vol. 44, No. 7, pp. 1037-1040.

[16] Barrio, R. A., Galeener, F. L., Martinez, E., (1984) "Vibrational Bethe Lattice With Random Dihedral Angles," Physical Review Letters, Vol. 52, No. 20, pp. 1786-1789.

[17] Sharma, S. K., Mammone, J. F., Nicol, M. F., (1981) "Raman Investigation of Ring Configurations in Virteous Silica," Nature, Vol. 292, pp. 140-141.

[18] Umari, P., Pasquarello, A., (2002) "Modeling of the Raman Spectrum of Virteous Silica: Concentration of Small Ring Structures," Physica B 316-317, pp. 572-574.

[19] Sarnthein, J., Pasquarello, A., Carr, R., (1995) "Model of Virteous SiO2 by ab initio Molecular-Dynamics Quench From the Melt," Physical Review B, Vol. 52, No. 17 12690-12695

[20] Vashishta, P., Kalia, R. K., Rino, J. P. (1990) "Interaction Potential for SiO_2: A Molecular-Dynamics Study of Structural Correlations," Physical Review B, Vol. 41 No. 17 pp. 12197-12209.

[21] Meier, R. J., (2005) "On Art and Science in Curve-Fitting Vibrational Spectra," Vibrational Spectroscopy 39, pp. 266-269.

[22] Chan, J.W., Huser, T., Risbund, S., Krol, D.M., (2001) "Structural Changes in Fused Silica After Exposure to Focused Femtosecond Laser Pulses," Optics Letters, Vol. 26 No. 21, pp. 1726-1728

[23] Miura, K., Qiu, J., Inouye, H., Mitsuyu, T., Hirao, K., (1997) "Photowritten Optical Waveguides in Various Glasses with Ultrashort Pulse Laser," Applied Physics Letters 71 (23), pp. 3329-3331

[24] Bellouard, Y., Colomb, T., Depeursinge, C., Said, A. A., Dugan, M., Bado, P., (2006) "Investigation of Femtosecond Laser Irradiation on Fused Silica," Proc. Of SPIE Vol. 6108M

[25] Glezer, E. N., Milosavljevic, M., Huang, L., Finlay, R. J., Her, T.-H,. Callan, J. P., Mazur, E., (1996) "Three-Dimensional Optical Storage Inside Transparent Materials," Optics Letters, Vol. 21, No. 24,, pp. 2023-2025

[26] Glezer, E. N., Mazur, E., (1997) "Ultrafast-Laser Driven Micro-Explosions in Transparent Materials," Applied Physics Letters, 71 (7), pp. 882-884

[27] Schaffer, C. B., Brodeur, A., Garcia J. F., Mazur, E., (2001) "Micromachining Bulk Glass by Use of Femtosecond Laser Pulses with Nanojoule Energy," Optics Letters, Vol. 26, No. 2, pp 93-95

[28] Schaffer, C. B., Garcia J. F., Mazur, E., (2003) "Bulk Heating of Transparent Materials Using a High-Repetition-Rate Femtosecond Lasers," Applied Physics A 76, pp. 351-354.

[29] Schaffer, C. B., Jamison, A. O., Mazur, E., (2004) "Morphology of Femtosecond Laser-Induced Structural Changes in Bulk Transparent Materials," Applied Physics Letters, Vol. 84 No. 9, pp. 1441-1443.

[30] Watanabe, W., Onda, S., Tamaki, T., Itoh, K., (2007) "Direct Joining of Glass Substrates by 1 kHz Femtosecond Laser Pulses," Applied Physics B, 87, pp. 85-89.

[31] Watanabe, W., Onda, S., Tamaki, T., Itoh, K., Nishii, J., (2006) "Space-selective Laser Joining of Dissimilar Transparent Materials Using Femtosecond Laser Pulses," Applied Physics Letters 89, pp. 1-3.

[32] Tamaki, T., Watanabe, W., Nishii, J., Itoh, K., (2005) "Welding of Transparent Materials Using Femtosecond Laser Pulses," Japanese Journal of Applied Physics, 44, pp. L687-L689.

[33] Kucheyev, S. O., Demos, S. G., (2003) "Optical Defects produced in Fused Silica During Laser-Induced Breakdown," Applied Physics Letters, Vol.82, No. 19, pp. 3230-3232.

[34] Stuart, B. C., Feit, M. D., Rubenchik, A. M., Shore, B. W., Perry, M. D., (1995) "Laser-Induced Damage in Dielectrics with Nanosecond and Subpicosecond Pulses," Physical review Letters, Vol. 74 No. 12, pp. 2248-2251

[35] Sushchinskii, M. M., (1972) Raman Spectra of Moleculs and Crystals, Keter Publishers Ltd., London

[36] Fuxi, G., (1992) Optical and Spectroscopic Properties of Glass, Springer-Verlag, New York

[37] Reichman, W. J., Krol, D. M., (2006) "A Spectroscopic Comparison of Femtosecond-Laser-Modified Fused Silica Using Kilohertz and Megahertz Laser Systems," Journal of Applied Physics 99, pp. 99-99

[38] Reichman, W. J., Chan, J. W., Krol, D. M., (2003) "Confocal Fluorescence and Raman Microscopy of Femtosecond Laser-Modified Fused Silica," Journal of Physics: Condensed Matter 15 pp. S2447-S2456

[39] Galeener, F. L., (1979) "Band limits and the vibrational spectra of tetrahedral glasses," Physical Review B, Vol. 19, No. 8, pp. 4292- 4297.

[40] Miyamoto, I., Horn, A., Gottmann, J., Wortmann, D., Yoshino, F., (2006) "High-precision, High-throughput Fusion Welding of Glass Using Femtosecond Laser Pulses," Proceedings of the 4th International Congress on Laser Advanced Materials Processing, Kyoto Research Park, Kyoto, Japan